# Illuminating a bacterial adaptation mechanism: infrared-driven cell division in deep-sea hydrothermal vent environments

Jie Dai, Xue-Gong Li, Tian-Yuan Zhang, Hong Chen, Wei-Jia Zhang, Denghui Li, Jia Liu, Jianwei Chen, Yuan Lu, Long-Fei Wu

ARTICLE



# Illuminating a bacterial adaptation mechanism: Infrared-driven cell division in deep-sea hydrothermal vent environments

Jie Dai,[1,10] Xue-Gong Li,[2,3,4,5,10] Tian-Yuan Zhang,[6] Hong Chen,[2,11] Wei-Jia Zhang,[2,3,4,5] Denghui Li,[5,7] Jia Liu,[8] Jianwei Chen,[7] Yuan Lu,[9] and Long-Fei Wu[1,3,*]

*Correspondence: wu@imm.cnrs.fr

Received: November 21, 2023; Accepted: January 30, 2024; Published Online: February 21, 2024; https://doi.org/10.59717/j.xinn-geo.2024.100050



## GRAPHICAL ABSTRACT

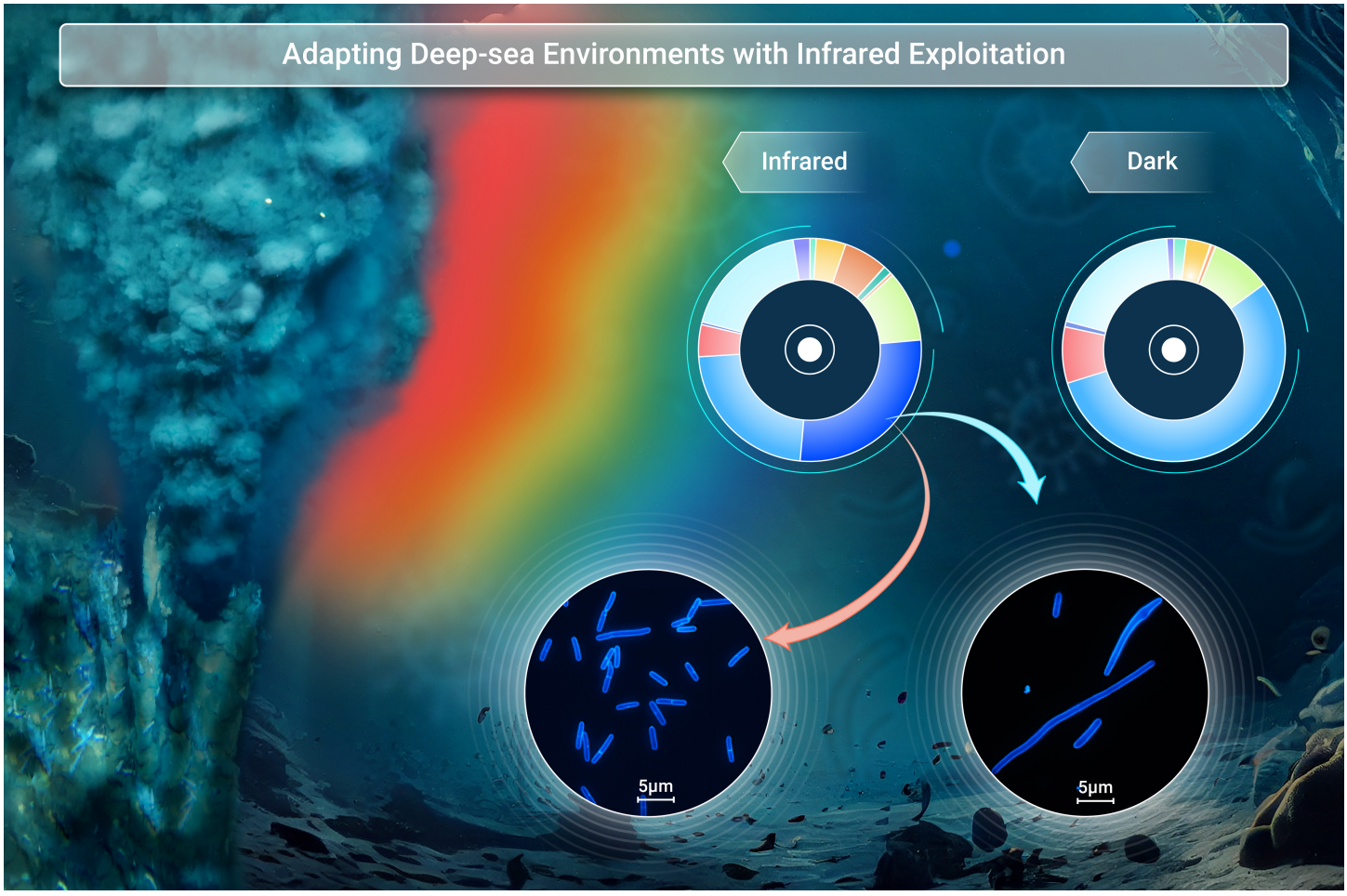


## PUBLIC SUMMARY

- The infrared (IR) radiation from hydrothermal vents impacted the composition of the microbial population.
- A deep-sea bacterial strain was isolated from cultures enriched through IR irradiation.
- High hydrostatic pressure (HHP) hindered bacterial peptidoglycan (PG) synthesis and cell division.
- IR irradiation triggered PG synthesis and cell division under HHP, promoting bacterial growth.

ARTICLE

www.the-innovation.org/geoscience

# Illuminating a bacterial adaptation mechanism: Infrared-driven cell division in deep-sea hydrothermal vent environments

Jie Dai,[1,10] Xue-Gong Li,[2,3,4,5,10] Tian-Yuan Zhang,[6] Hong Chen,[2,11] Wei-Jia Zhang,[2,3,4,5] Denghui Li,[5,7] Jia Liu,[8] Jianwei Chen,[7] Yuan Lu,[9] and Long-Fei Wu[1,3,*]

[1]Aix Marseille University, CNRS, LCB, IMM, CENTURI, Marseille 13000, France
[2]Laboratory of Deep-Sea Microbial Cell Biology, Institute of Deep-sea Science and Engineering, Chinese Academy of Sciences, Sanya 572000, China
[3]International Associated Laboratory of Evolution and Development of Magnetotactic Multicellular Organisms, CNRS-Marseille/CAS-Sanya, Sanya 572000, China
[4]CAS Key Laboratory for Experimental Study under Deep-sea Extreme Conditions, Institute of Deep-sea Science and Engineering, Chinese Academy of Sciences, Sanya 572000, China
[5]Institution of Deep-sea Life Sciences, IDSSE-BGI, Hainan Deep-sea Technology Laboratory, Sanya 572000, China
[6]Aix Marseille University, CRCM, INSERM, CNRS, Marseille 13000, France
[7]Qingdao Key Laboratory of Marine Genomics, BGI Research, Qingdao 266000, China
[8]CAS Key Laboratory of Marine Ecology and Environmental Sciences, Institute of Oceanology, Chinese Academy of Sciences, Qingdao 266000, China
[9]College of Physics and Optoelectronic Engineering, Ocean University of China, Qingdao 266000, China
[10]These authors contributed equally
[11]State Key Laboratory of Microbial Metabolism, School of Life Sciences and Biotechnology, Shanghai Jiao Tong University, Shanghai 200240, China
*Correspondence: wu@imm.cnrs.fr

Received: November 21, 2023; Accepted: January 30, 2024; Published Online: February 21, 2024; https://doi.org/10.59717/j.xinn-geo.2024.100050



Citation: Dai J., Li X.G., Zhang T.-Y., et al., (2024). Illuminating a bacterial adaptation mechanism: Infrared-driven cell division in deep-sea hydrothermal vent environments. The Innovation Geoscience **2(1)**: 100050.

Based on Planck's black-body radiation law, deep-sea hydrothermal vent chimneys emit light, predominantly infrared light, which potentially supports bacterial photosynthesis in this ecosystem independently of the solar energy. To investigate the impact of this geothermal light on bacterial growth, we collected samples from the Southwest Indian Ridge and demonstrated that infrared light alone promotes bacterial growth and alters population composition. The mechanism of infrared stimulated growth was analyzed by monitoring cell wall synthesis using the *Tepidibacter hydrothermalis* strain SWIR-1, which was isolated from cultures enriched through infrared irradiation. The results showed that the elevated hydrostatic pressure inhibited septal peptidoglycan synthesis and cell division, but had less effect on cell elongation, chromosome replication and segregation. The dominant cell shape was filaments with some swelling and inertness in cell wall synthesis depending on the level of pressure applied. Interestingly, irradiation with 880 nm infrared light effectively initiated septal synthesis and alleviated the obstruction. This revelation uncovers a novel adaptation mechanism involving infrared light for bacteria dwelling in deep-sea environments, and sheds light on the potential of infrared-mediated photobiomodulation.

## INTRODUCTION

The hydrostatic pressure in the ocean increases with depth due to the accumulating weight of the water column. At the sea surface, the hydrostatic pressure is approximately 0.1 MPa (megapascals). The pressure rises by about 1 MPa for every additional 100 meters of depth. The deep sea, referred to as the zone with depths exceeding 1,000 meters, constitutes a cold, dark, and oligotrophic environment characterized by high hydrostatic pressure (HHP, > 10 MPa).[1]This elevated pressure significantly impacts bacterial physiology, influencing aspects such as metabolism, gene expression and protein structure and function.[2,3]Bacteria may counteract the detrimental effects of HHP by adjusting their membrane composition to maintain membrane integrity, producing pressure-resistant enzymes, or enhancing the efficiency of existing enzymes to sustain crucial metabolic reactions. Moreover, in response to deep-sea pressure, bacteria modify their gene expression patterns, activating specific genes involved in stress response, DNA repair, and cellular structure maintenance.[2,4-6] In addition, HHP generally impairs cell growth and division. In 1950, Zobell and Oppenheimer conducted a comprehensive analysis of the impact of HHP on marine bacteria, discovering that the growth of most of the analyzed bacteria was inhibited by pressures ranging from 20 to 60 MPa. However, certain barophilic (now referred to as piezophilic) variants from deep-sea environments managed to thrive even under higher pressures. These specific piezophilic bacteria exhibited elongated cells and unusual morphological shapes under HHP. For instance, *Serratia marinorubra* showed an increase in size without signs of division at pressures ranging from 40 to 60 MPa.[7]In comparison, non-marine model strain *Escherichia coli* experienced inhibited growth and reproduction between 10 and 50 MPa. Additionally, HHP caused longer cell filaments and disrupted cell division, which was linked to reduced DNA replication.[8]Another study has demonstrated that elevated pressure (40 MPa) inhibited the formation of FtsZ-rings in *E. coli*, resulting in elongated filamentous cells.[9]However, the mechanisms by which bacteria adapt to the effects of HHP on cell division remain not fully understood.

In deep oceans, hydrothermal vents expel superheated, anoxic, chemical-rich fluids into the cold, oxic, deep ocean. Specialized bacteria and archaea adeptly convert these chemical-rich compounds into nourishment that sustains life, a process aptly known as chemosynthesis.[10,11]Remarkably, black chimneys with temperatures reaching 360-400 °C emit light, predominantly infrared (IR) light, which has been hypothesized to have played a pivotal role in the evolution of photosynthesis within hydrothermal vent ecosystems.[11-15] In fact, an aerobic phototrophic Alphaproteobacterium strain and a strictly anaerobic photosynthetic green sulfur bacterium strain were isolated from the plume waters of black smokers at the Juan de Fuca Ridge and the East Pacific Rise, respectively.[16,17]Intriguing questions arise regarding the prevalence of phototrophs in deep-sea hydrothermal vents, encompassing geographical and taxonomical aspects, combined with the consequential impact of IR on microorganism life. To explore these questions, we collected samples from hydrothermal vents in the Longqi field on the ultraslow-spreading Southwest Indian Ridge (SWIR) during the TS10 expedition from December 2018 to February 2019. Our metagenomic analysis has unveiled a complete chlorophyll biosynthesis pathway and genes encoding rhodopsin in these samples,[18]implying an underestimated influence of geothermal light on life within the chemosynthetic hydrothermal ecosystems. The extent to which microorganisms exploit IR light in their adaptation to the enigmatic deep-sea hydrothermal ecosystems remains poorly understood. This study demonstrated that IR light alone can effectively stimulate bacterial growth and alter the composition of the microbial community. Additionally, it was observed that HHP impairs septal peptidoglycan (PG) synthesis and cell division, while allowing cell elongation. Interestingly, IR light triggers cell wall synthesis at the septum, thereby alleviating the inhibition of cell division induced by HHP.

## MATERIALS AND METHODS

### Cultivation, Fluorescent D-amino acid (FDAA) labeling and microscope observation of SWIR-1 cells

The growth media used in this study were DSMZ 1040 (also called SRB, for $l^{-1}$ distilled water: 35 g Sea Salt (SIGMA), 1 ml Wolfe's mineral elixir, 1 g yeast extract, 0.5 ml sodium resazurin (0.1% w/v), 1 g $Na_2CO_3$, 2.5 g Na-DL-lactate, 1 ml Wolin's vitamin solution (10x), 0.3 g $Na_2S{\cdot}9\ H_2O$), and TRM medium (for

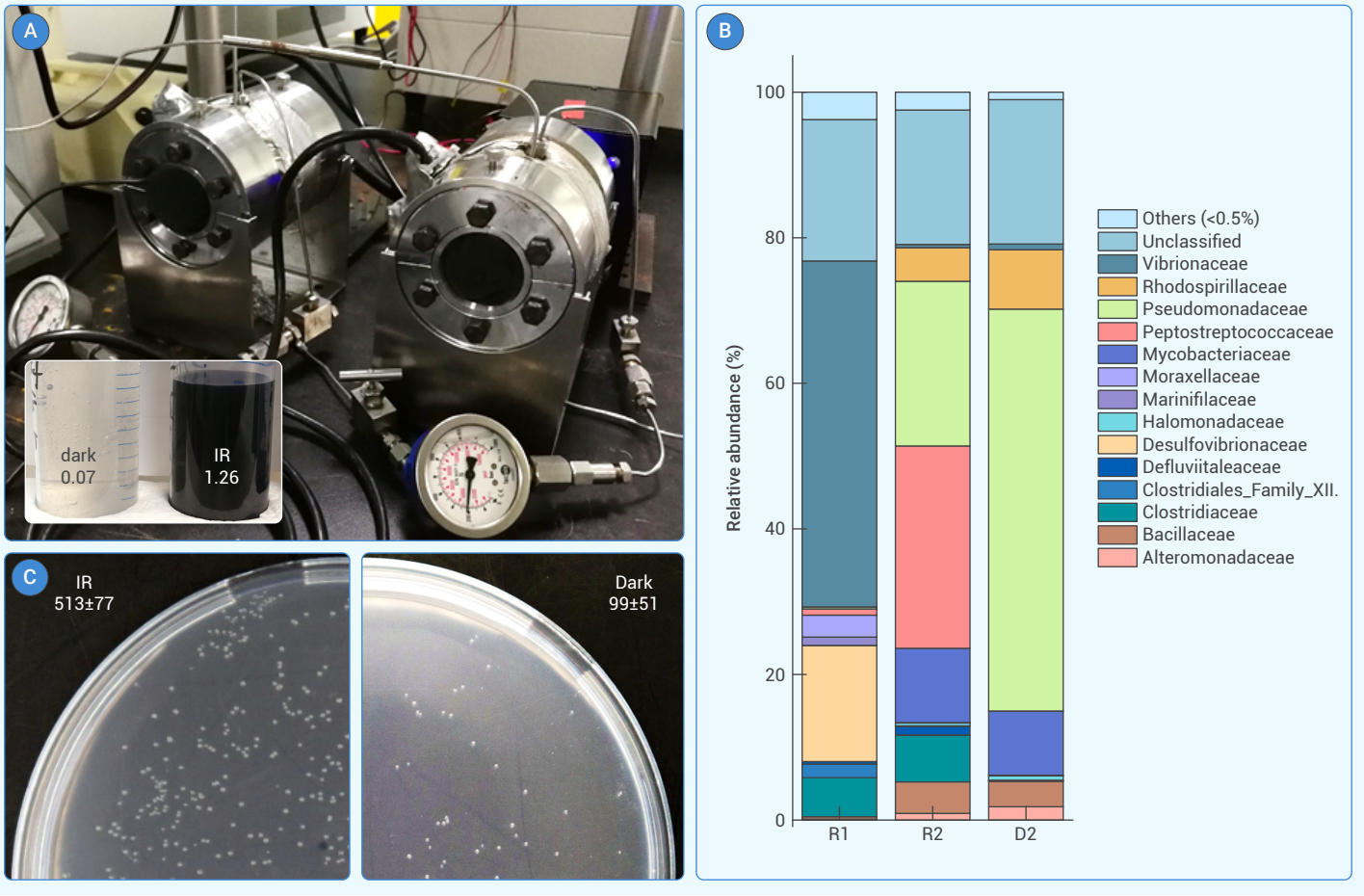


**Figure 1. IR stimulated the growth of hydrothermal vent microorganisms** (A) Custom-made high-pressure, high-temperature, light-illumination incubator (HPI) allowed IR boosting vent microbe growth as shown in the inlet with the cultures and their optical density. (B) shows the population composition of the cultures obtained on board with IR irradiation (R1) and subsequent re-inoculations in the laboratory with IR irradiation (R2) or in darkness (D2). (C) IR-enriched culture was incubated on plates with IR irradiation or in dark. The average number and the standard deviation of colonies from 5 plates for each condition are shown.

$l^{-1}$ distilled water 23 g NaCl, 5 g $MgCl_2{\cdot}6H_2O$, 0.7 g KCl, 0.5 g $(NH_4)_2SO_4$, 0.06 g $KH_2PO_4$, 0.06 g $K_2HPO_4$, 0.05 g NaBr, 0.02 g $CaCl_2{\cdot}2H_2O$, 0.01 g $SrCl_2{\cdot}6H_2O$, 6.75 mg $FeCl_3{\cdot}6H_2O$, 4 g tryptone, 1 g yeast extract, 3.3 g PIPES and 1.0 mg resazurin) were used. Anaerobic cultures were conducted in serum bottles closed with butyl rubber stoppers. Dissolved oxygen was removed by pumping vacuum and bubbling nitrogen repeatedly, and the bottles were subsequently sterilized by autoclaving at 121 °C for 20 min. The sterile $Na_2S{\cdot}9H_2O$ stock solution was added with a final concentration of 0.1% (w/v) before inoculation.

On board, 20 ml each of diffuse flow sample from a decompressurized high-pressure bottle (HPB) conserved at 4 °C was inoculated into 80 ml of SRB medium in a 100 ml bottle. The bottle was kept at room temperature (25 °C) with illumination by room tungsten light. After a 10-day incubation, the color of the SRB medium in the bottle changed from pink to translucid, and spectrophotometry analysis and microscope observation indicated bacterial growth. The SRB tungsten-enriched culture was inoculated in TRM media, and transferred to the high-pressure illumination cylindrical incubators (HPI, Figure 1A), which were pressurized to 30 MPa and incubated at 30 °C. One HPI was kept in the dark, while the other was irradiated with 880 nm IR light-emitting diode (LED) on one side and another 940 nm LED on the opposite side of the incubator to enrich piezophilic or piezotolerant phototrophs. After a 7-day incubation, the culture that had been boosted by IR was conserved in 30% glycerol at -80 °C. Back to the laboratory, 2 × 2 ml each of the -80 °C conservation were inoculated in TRM media in HPIs or serum bottles and incubated as indicated.

Strain SWIR-1 was routinely grown in the 904aVT medium, which contains ($l^{-1}$ distilled water) 23 g NaCl, 5 g $MgCl_2{\cdot}6H_2O$, 0.7 g KCl, 0.5 g $(NH_4)_2SO_4$, 0.06 g $KH_2PO_4$, 0.06 g, $K_2HPO_4$, 0.02 g $CaCl_2{\cdot}2H_2O$, 6.75 mg $FeCl_3{\cdot}6H_2O$, 4 g MES, 1 g yeast extract, 1 g tryptone, 1 g L-cysteine-$HCl{\cdot}H_2O$, and 1.0 mg resazurin.[19]Dissolved oxygen in the medium was replaced by nitrogen as described above. The prepared medium was sterilized by autoclaving at 121 °C for 15 min. After cooling, 10 ml of 25% (w/v) glucose and 10 ml of vitamin solution (see JCM Medium No. 141) from anaerobic sterile stock solutions were added into the medium. 10 ml of 10% (w/v) $Na_2S{\cdot}9H_2O$ from anaerobic sterile stock solutions were added before inoculation. The 904aVT plate was prepared by adding 1.5% (w/v) agar before autoclaving. Cell morphology was routinely inspected using Zeiss Axiostar plus microscope.

For fluorescent D-amino acid (FDAA) labeling, strain SWIR-1 was inoculated into 904aVT media containing 0.2 – 0.25 mM FDAA (Bio-techne, France). After the specified duration of incubation, cells were harvested, fixed with 1% paraformaldehyde (PFA) at room temperature for 20 minutes, and then washed three times with PBS buffer. The cells were subsequently observed using a Nikon ECLIPSE Ti microscope.

To assess the impact of HHP and light exposure on cell growth with FDAA labeling, we utilized devices with smaller culture volumes compared to HPI. Precultures were inoculated in fresh 904aVT media containing a single-color FDAA, followed by a nitrogen flush and subsequent filling of 3 ml serum bottles within an anaerobic chamber. These serum bottles were then placed in a High-Pressure Spectrophotometer analysis cell (HPS, PCI500, Syn-Corporation, Kyoto, Japan) and pressurized to 30 MPa. The HPS was illuminated with LED light through the optical windows of the HPS and incubated at 25 °C for a specified time. In parallel, another set of serum bottle was incubated in an HPB in darkness at 30 MPa and 25 °C. A thermostatic water circulation was connected to HPS, whereas the HPB was placed in the same water bath to maintain the same temperature. After a 20-minute incubation period, the cultures were depressurized, and the cells were harvested. Subsequently, the cells were washed three times with fresh media and resuspended in fresh media containing FDAA of a different color compared to the

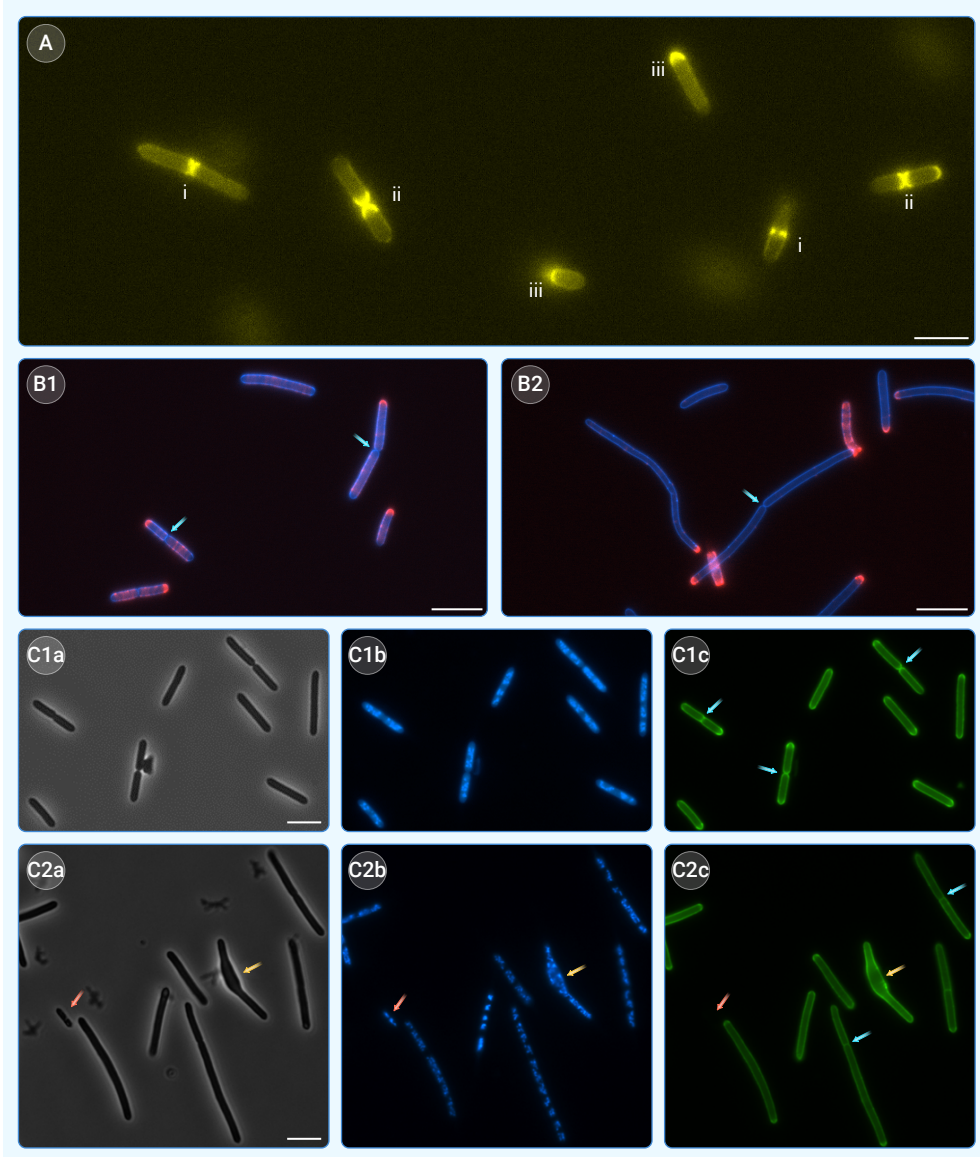


**Figure 2. HHP affected SWIR-1 PG synthesis and cell division** (A) YADA at 0.2 mM was incorporated in PG mesh of SWIR-1 cells incubated in dark at 0.1 MPa at 30°C. (B) Pulse-chase double labeling through initial label by RADA at 0.1 MPa, and subsequent label by HADA and incubation at 0.1 MPa in B1 and 30 MPa in B2. Cyan arrows show the septa. Phase contrast images (C1a and C2a), DAPI (blue, C1b and C2b) and sBADA (green, C1c and C2c) stained SWIR-1 cells were incubated at 0.1 MPa (C1) and 30 MPa (C2) in darkness at 30°C. Cyan arrows show the septa, yellow arrow points to deform cell and pink arrow shows the PG synthesis inert cell. Scale bars: 5 μm.

initial labeling. The cultures were pressurized accordingly, and incubated with or without IR irradiation. At the indicated times, cells were harvested and prepared for observation. Alternatively, cultures were transferred into a syringe, which was then inserted into an HPB equipped with a piston. The cultures were injected into a High-Pressure Microscope Observation Unit (HPOU, PMC-100, Syn-Corporation, Kyoto, Japan) using a manual pump. The HPOU was pressurized and kept connected to the HPB to maintain pressure throughout the experiment. The HPOU was mounted onto the ZEISS Observer A1 microscope (ZEISS, France) and illuminated with Thorlabs LED (Thorlabs, France) at the specified wavelength. It is worth noting that the culture within the tube and syringe remained in the dark condition during these procedures. Temperature monitoring within the HPOU and HPB was conducted using Thorlabs TSP01 temperature sensors

### Illumination system

Thorlabs (Thorlabs, France) mounted LEDs M880L3 and M970L4 were used to illuminate the SWIR-1 cultures. The power of these LEDs was measured using a Thorlabs power meter (PM100D) equipped with the S120C sensor, positioned at the level of the window of either the HPS or HPOU.

### Image analysis

The phase-contrast images and the fluorescent images were converted from ND2 format to TIFF format using ImageJ software (https://imagej.net/ij/). To provide a more comprehensive description and statistical analysis of cell size, morphology, and division septa, we implemented a high-throughput analysis tool, referred to as "SSCA" (segmentation-skeletonization-classification-analysis), coded through Python, which allows automatic identification and quantification of these factors in image datasets. Bacterial segmentation and mask construction were performed using Omnipose, a deep neural network image-segmentation algorithm with pre-trained models that generate a binary mask from the phase-contrast image for each cell.[20] Then, we used a Python package FilFinder to extract the skeleton, also referred to as medial axis, of rod-shaped bacteria.[21] The dimensions (width, length and area) of each bacterium were calculated based on its skeleton. A conversion rate of 1 μm to 15.56 pixels was applied. To calculate the fluorescence intensity of the bacteria, binary masks from the phase-contrast image were used in combination with the corresponding fluorescent image. Fluorescence intensity was determined using the formula Y= 0.212R + 0.701G + 0.087B. When the average fluorescence intensity of a cell Y' was greater than 0.1, the bacteria were labeled, as well as to determine the position of FDAA insertion in the PG network. The high fluorescence foci of each cell were identified and calculated for width on both sides along the central skeleton line by each pixel. We used find_peaks from the Scipy package to identify cell morphology and PG synthesis in 1-D array.[22] After observation and test, prominence=0.3 and wlen=20 for finding width peaks, prominence=0.02 and wlen=8 for finding fluorescence peaks. Based on the peak analysis, we classified cells into 8 categories as shown in Figure 6.

### Gene context analysis

The context conservation of interesting genes were analyzed and visualized using GeCoViz,[23] which uses precomputed information on orthology assignments, phylogenetic information and functional annotations for over 42 million genes extracted from 12,221 reference prokaryotic genomes.

## RESULTS

### IR stimulated vent bacterial growth and altered population composition

During the dive SY111 of the manned submersible *Shen Hai Yong Shi* to the active vent DFF18 (37° 46' 51.60" S, 49° 38' 52.44" E) at the depth of 2,700 m, diffuse flow (9.2 °C) close to a black smoker venting (330 °C) was collected using pressure-conserving sterilized sampling bottle (HPB, Top Industry, Paris, France). The HPB was opened only on site by the manipulator of the manned submersible to avoid contamination from other places. On board, piezophile or piezotolerant and phototrophic microorganisms were enriched using specifically designed and custom-made HPI under high pressure (30 MPa, Materials and methods) (Figure 1A). One incubator was kept in

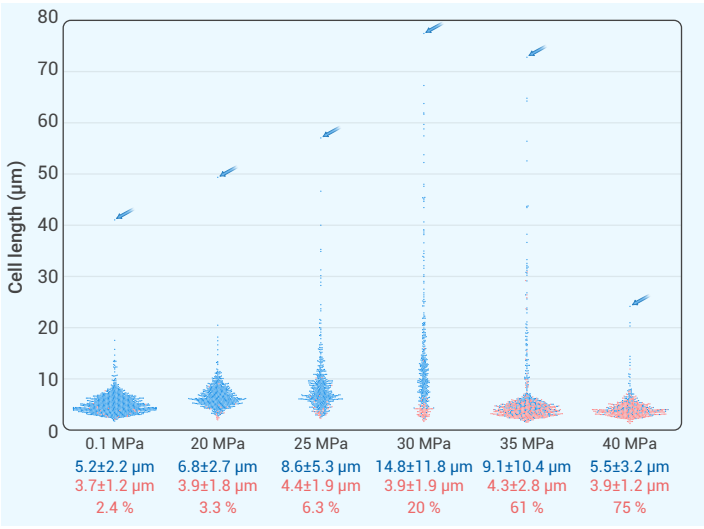


**Figure 3. Effect of HHP on FDAA incorporation and cell division** The SWIR-1 cells were incubated under different pressures at 30°C in the dark. Actively labeled cells and inert non-fluorescent cells appear as blue and red symbols in the swarm plot, respectively. Their median sizes with SD are indicated by corresponding blue and red numbers. The percentage (%) indicated inert cells observed. Blue arrows denote maximal filament sizes.

the dark, while another was irradiated with IR LEDs of 880 nm and 940 nm on the incubator to mimic the light emitted by the black chimneys in Longqi hydrothermal vent field, as detected. After a 7-day incubation, the absorption at 600 nm was 1.26 for IR-culture and 0.07 for the dark-culture (Figure 1A, inset), indicating an IR stimulated growth. The black color disappeared upon exposure to air, suggesting the production of FeS, as is often observed with marine anaerobic cultures. The IR-culture and membranes containing filter-collected cells were conserved at -80 °C for later analysis. The dark-culture did not grow and the biomass was insufficient for further analysis.

Back to the laboratory, the conserved sample was inoculated and incubated at 30 MPa in HPIs or 0.1 MPa in anaerobic serum bottles with 880 and 940 nm irradiation or in the dark. After 70 h incubation in HPI, the cultures under HHP with IR irradiation (designated as R2) and in darkness (D2) reached 0.43 and 0.09 of absorption density at 650 nm, respectively. The counterparts of the cultures at 0.1 MPa were 0.08 with IR irradiation and 0.03 in darkness. The mixed population displayed a piezophilic phenotype. The results indicated that HHP and IR irradiation stimulated the growth of the culture. Metagenomic analysis showed that Peptostreptococcaceae was the most abundant population in R2, while being among the lowest families in D2, where Pseudomonadaceae emerged as the predominant group (Figure 1B). Therefore, IR altered the population composition of the cultures.

Cultures incubated at elevated pressure with IR irradiation were diluted and spread onto TRM plates. Half of the cultures were incubated under IR irradiation, while the other half were incubated in the dark. Interestingly, the number of colonies obtained from the light-illuminated plates was approximately five times higher than that from the dark plates (Figure 1C). Five colonies were picked up from the plate irradiated by IR and found to belong to the *Tepidibacter* genus of the family Peptostreptococcaceae when analyzed by 16S rRNA gene amplification and sequencing. Subsequently, a pure culture designated as strain SWIR-1 was obtained after streaking out. The genome of strain SWIR-1 was sequenced, revealing a 4.12 Mb circular chromosome consisting of 3,861 protein-coding sequences with 29.25% GC content and a plasmid of 38,843 bp. Average nucleotide identity (ANI) and in silico digital DNA-DNA hybridization (dDDH) analyses, when compared to reference strains *Tepidibacter mesophilus* B1$^T$, *Tepidibacter fomicigenes* DV1184$^T$, and *Tepidibacter thalassicus* SC562$^T$, classified the isolate SWIR-1 as a novel species within the genus *Tepidibacter*. It was named *Tepidibacter hydrothermalis* SWIR-1 [19,24]. To understand the mechanism of IR irradiation stimulated growth, we analyzed the genome of SWIR-1. Genes encoding neither chlorophyll synthesis nor rhodopsin were detected. Therefore, it seems that IR irradiation promotes cell growth through unknown mechanisms.

## HHP hindered SWIR-1 PG synthesis and cell division

The initial culture of a mixed population exhibited better growth at 30 MPa compared to 0.1 MPa, indicating a piezophilic phenotype. The strain SWIR-1 axenic culture was isolated on plates at 0.1 MPa, the effect of HHP on its growth was further analyzed by inspecting PG synthesis and cell morphology. In rod-shaped bacteria, growth typically involves the elongation of cell bodies, followed by division at the mid-cell to generate two identical progenies. Elongation is facilitated by the elongasome protein complex comprising MreB, RodA, and PBP2, which carries out dispersed synthesis of PG in the side walls of cells.[25]In contrast, the divisome consisting of key players FtsZ, FtsW, and FtsI, synthesizes PG zonally at the septa. PG is a net-like layer that surrounds the cell membrane and precisely determines cell size and shape. The macromolecular polymer PG is composed of β-1,4-linked glycan strands cross-linked by short D-amino acid (DAA)-containing peptide chains. FDAAs can be efficiently incorporated at the sites of PG biosynthesis, allowing for specific and covalent probing of bacterial growth with minimal disruption.[26]

Bacterial growth occurs when the PG cell wall enlarges and divides. Precursors are incorporated into the existing PG network at specific locations over a defined period of time. FDAAs with varying characteristics, including size, solubility, photo- and thermostability, as well as fluorescent spectra (such as blue HADA, green sBADA, red RADA, and yellow YADA[27]) were efficiently integrated into the side walls and septa of SWIR-1 cells when incubated at 0.1 MPa (Figure S1).

A brief YADA labeling revealed PG synthesis at the mid-cell (Figure 2A, i), septa (ii), and one cell pole (iii), suggesting active PG synthesis during cell division. To gain more details about the PG synthesis process, pulse-chase double labeling experiments were conducted. After an initial red RADA labeling at 0.1 MPa for 1 hour, cells were washed and labeled with blue HADA in the dark, either at 0.1 MPa for 1 h (Figure 2B1) or under HHP for 17 h (Figure 2B2).

At 0.1 MPa, approximately 80% of the short-rod cells exhibited a pole with red fluorescence, indicating dominant RADA incorporation at one pole that remained unchanged during the long-time labeling. This old pole was inert during the elongation and growth. Furthermore, red stripes were observed in some cells, with an increasing density from the old red pole towards the incipient blue pole (Figure 2B1). The labeling pattern of RADA suggests that old PG is regularly removed though dispersed zonal opening, followed by de novo incorporation of blue HADA during the elongation of PG synthesis starting from the old pole.

Under elevated pressure, most cells (80%) appeared as long filaments with a inert red pole and a periphery blue halo without red stripes (Figure 2B2). The morphology suggests efficient de novo elongation synthesis of PG with no septal formation. The red stripes were observed only in short cells, approximately 5 μm in length. These results imply that initial red PG was removed, but there was no significant de novo PG synthesis and cell elongation in these short cells.

The application of HHP resulted in a filamentous morphology, which raises the question of whether elevated pressure affects DNA replication in SWIR-1. SWIR-1 cells exhibited a median size slightly exceeding 5 μm under 0.1 MPa (Figure 2C1). Septa effectively divided cells into two offspring, often possessing two DAPI-stained chromosome zones in each cell (Figure 2C1b-C1c). In contrast, cells subjected to HHP at 25 MPa in darkness elongated into filamentous structures (Figure 2C2) with multiple DAPI-stained zones (Figure 2C2b). However, these filaments lacked well-defined septal separation (Figure 2C2c). The impact of HHP was primarily observed in PG synthesis at the septa, with no apparent effect on chromosome replication or segregation. Notably, the phase microscope revealed the presence of short cells (pink arrow in Figure 2C2) with visible chromosomes, as shown in Figure 2C2b. However, these cells were not labeled by FDAA (Figure 2C2c), suggesting their inactivity or death while maintaining their initial size and chromosome morphologically intact. Additionally, certain cells displayed an inflated or swollen morphology (yellow arrow in Figure 2C2).

The impact of HHP on SWIR-1 cell PG synthesis, division, and mortality was further investigated (Figure 3). Analysis of cell length distribution revealed that the median size of HADA-labeled cells actively increased from 5.2 μm at 0.1 MPa to 14.8 μm at 30 MPa, then subsequently decreased to 5.5 μm at 40 MPa. The proportion of filamentous cells followed a similar trend in

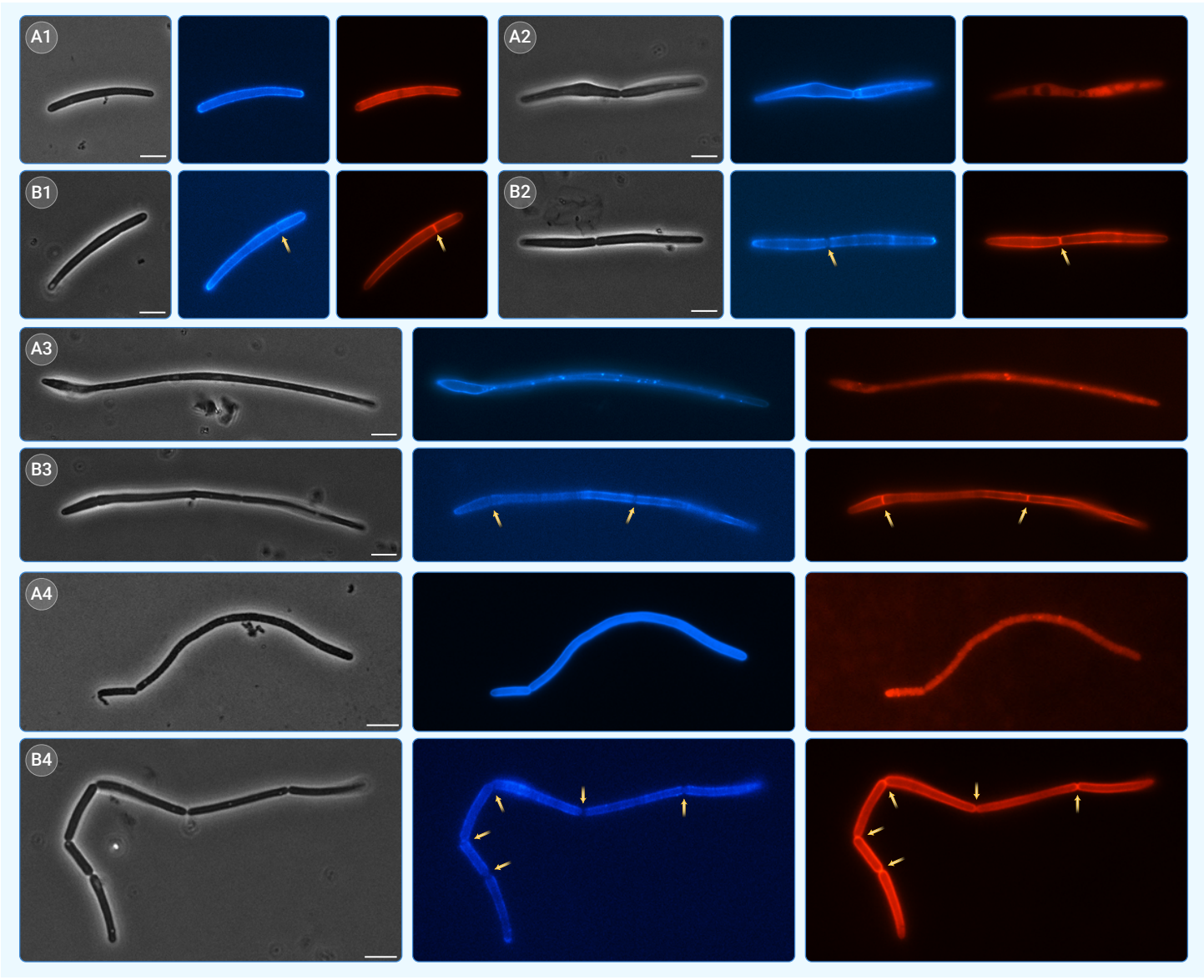


**Figure 4. IR triggers PG synthesis at septa** The cells were initially incubated with HADA (blue fluorescence) at 30 MPa in darkness for overnight. They were then collected, washed and resuspended in fresh media supplemented with RADA and incubated at 30 MPa in darkness (series A) or with 880 nm irradiation (series B) for 1h at 30 MPa. Yellow arrows show newly synthesized PG at septa. Scale bars: 5 μm.

response to the increasing pressure. The longest filamentous cell measured 77.4 μm at 30 MPa. Importantly, the percentage of inert cells, typically around 4 μm in size, escalated from 2.4% at 0.1 MPa to 20% at 30 MPa. As the pressure continued to be increased, the number of inactive cells became the majority, reaching 61% at 35 MPa and 75% at 40 MPa. This resulted in a progressive hindrance of cell division in SWIR-1 and an increased cell mortality rate with higher pressure. In contrast to the initial mixed population, the derived axenic culture SWIR-1 exhibited a pressure-tolerant phenotype.

## IR triggered PG synthesis at septa under HHP

Cell division was negatively impacted by elevated pressure, while IR irradiation promoted the growth of SWIR-1 cells. To better understand the effects of HHP and IR irradiation, we compared the cell morphology in cultures under HHP in darkness with those subjected to IR irradiation in HPS (Figure S2). The temperature was maintained at 25°C in all cultures. 18% of cells were actively labeled and filamentous, with a median size of 9.2 μm. The remaining 82% of cells were inactive with a short size of less than 5 μm when incubated in the dark. In cultures with IR irradiation, 98% of cells, were actively labeled and had a shorter size (5.1 μm). Abnormal cell shapes were observed mainly in the dark cultures.

A pulse-chase double labeling experiment was conducted on SWIR-1 cells. The cells were first incubated in the presence of blue HADA in darkness at 30 MPa overnight. Subsequently, the cells were collected, washed, and resuspended in fresh media containing red RADA. After that, the cells were incubated at 30 MPa for 1 hour in darkness (Figure 4, series A micrographs) or exposed to 880 nm IR irradiation (Figure 4, series B micrographs). The incorporation of HADA into the synthesized PG resulted in a halo of blue fluorescence on the cylindrical wall. Interestingly, the second labeling step revealed dispersed and irregular red fluorescence patterns, along with foci in some cases, in the cells that were subsequently incubated in darkness (series A, red panels). In contrast, IR irradiation induced not only peripheral PG synthesis, but also formation of the conspicuous septa (Figure 4, series B, indicated by yellow arrows). Compared to the sites of septa labeled in the second step by RADA, the blue labeling at these positions disappeared, indicating a dynamic removal of old PG and de novo synthesis of PG at the division sites. The result indicates that IR radiation triggers PG synthesis at septa and counteracts the inhibitory effect of HHP on cellular division.

## IR light at 880 nm efficiently improved the cell division of strain SWIR-1

To further evaluate the impact of HHP and light on the growth of SWIR-1, we designed a high-pressure cell growth analysis device (HPCG) (refer to Figure S3). The HPCG comprises a high-pressure observation unit (HPOU)

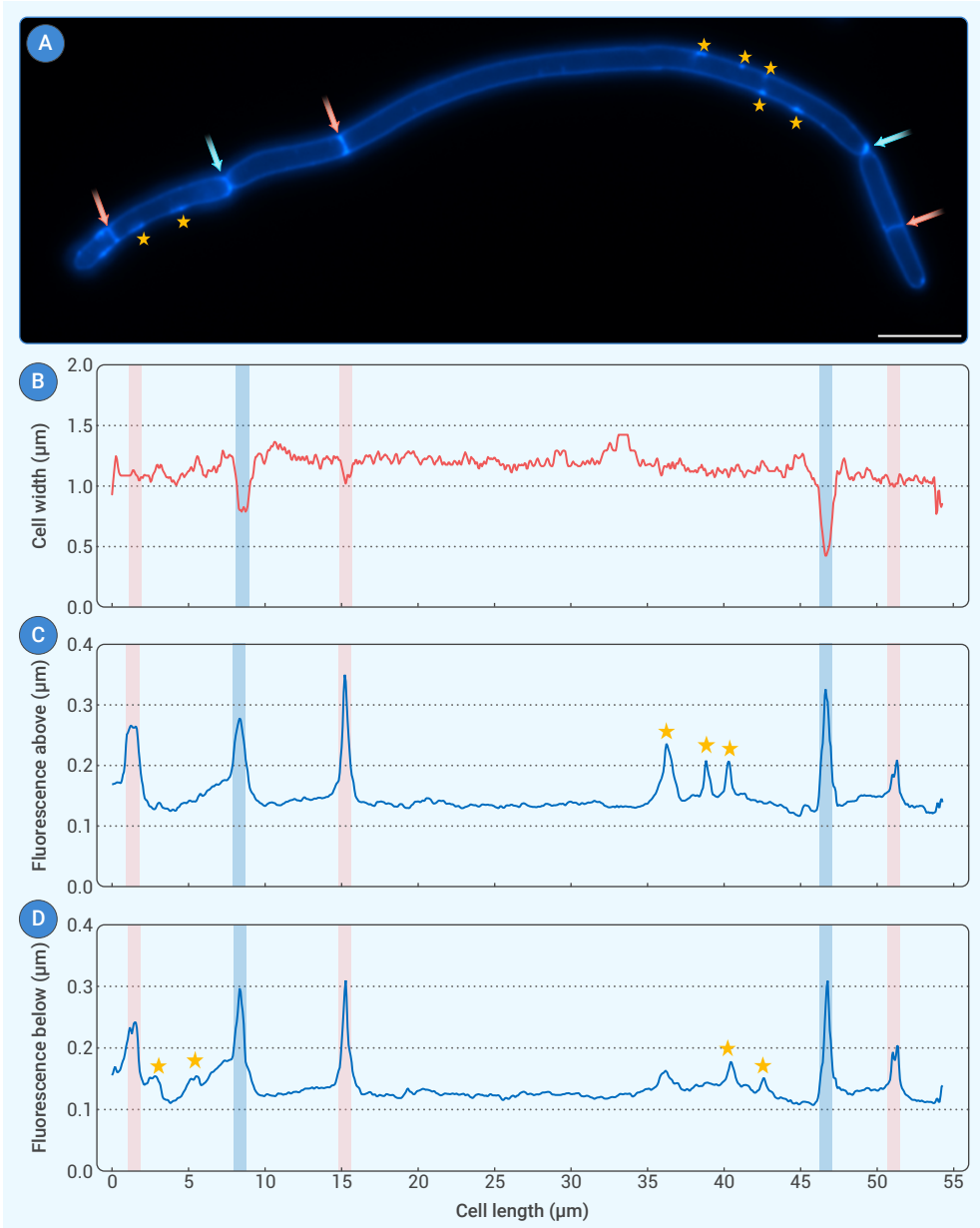


**Figure 5. Presentation of "SSCA" procedure used for high-throughput determination of cell size, fluorescence density and location** The phase contrast image was converted into mask image (This image is not displayed). The corresponding fluorescent image was superposed on the converted image (A). A skeleton in the center along the long cell axis was attributed and referred to as the medial axis. Based on the medial axis, the cell width was measured and plotted (B). The fluorescence intensity on the above or below medial axis was analyzed and plotted (C and D). The arrows indicated the septa with constriction (cyan arrows) and without (pink arrows). The yellow asterisks signify the fluorescence foci. Scale bars: 5 μm.

connected to a high-pressure bottle to maintain the pressure at a specific pressure level. Furthermore, an LED light with an appropriate lens was integrated onto a Zeiss microscope to illuminate the HPOU, and enable real-time observation of cells.

To efficiently analyze the images, we developed a high-throughput analysis tool for microscope image quantification, referred to as "SSCA" (Materials and methods). A medial axis (skeleton) along the long axis of a cell was established in binary masks generated from phase-contrast images. Using the medial axis as a reference, cell width (Figure 5B) and fluorescence above (Figure 5C) or below (Figure 5D) it was determined, as outlined in the Methods section. The constriction sites with FDAA-labeled septa were identified by positions with decreased cell width and increased fluorescence intensity symmetrically above and below the median axis (Figure 5A, cyan arrows; B-D, cyan highlight). Positions with clearly labeled FDAA septa but lacking cell wall constriction were indicated by pink arrows and highlighted in pink. Fluorescence foci above or below the median axis were automatically recognized and recorded (Figure 5, yellow asterisk).

SSCA enabled a comprehensive analysis of the impact of IR irradiation on cell growth and division. After 20 hours of incubation at 30 MPa and 24°C, under irradiation with an 880 nm LED at a radiance of 200 μW/cm² at the HPOU exit site, the system was depressurized. The cultures within the HPOU were collected as light-illuminated samples (L-samples), while those inside the unilluminated tube were labeled as dark samples (D-samples). The SWIR-1 cells were classified by SSCA into eight distinct patterns, five of which represent various stages of cell division.

The most prevalent pattern consisted of rod-shaped cells with peripheral halo fluorescence (Figure 6A1-2, panels La and Da), indicating cells in the process of elongation or just after division. These cells accounted for 70.1% of the population with a median size of 4.6 μm when exposed to IR (Figure 6A1, pattern La, and B1). In contrast, in darkness, these cells made up only 34.5% of the population, exhibiting a filamentous morphology with a median size of 11.3 μm (Figure 6A2, pattern Da, and B2). The second pattern showed cells initiating septum formation, as indicated by a single fluorescence spot in the middle of the cell (Lb and Db). This initiation led to the formation of a distinct septum band (panels Lc and Dc), followed by noticeable cell constriction (pattern 4, panels Ld and Dd), and culminating in pattern 5, where two offspring cells were observed (Le and De). Notably, in cells irradiated by IR, the division initiation site or septum was predominantly located at the mid-cell (Figure 6C1). However, in cells grown in the dark, it was found at various positions (1/4, 1/2, 3/4) or even irregular positions (C2). This suggests that SWIR-1 cells in darkness had difficulty in defining the normal division site.

Under IR irradiation, the proportion of cells exhibiting a single fluorescence spot (pattern b), the formation of a septum (pattern c), constriction of the cell wall (pattern d), and separation of progeny cells (pattern e) decreased from 16.1% to 5.5%, 3.9%, and 1.7%, respectively (Figure 6A1 and B1). This implies a smoother division process. In contrast, in darkness, the proportions of cells at the initiation step of division (pattern b with one fluorescence spot) and the formation of a septum (pattern c) were 22.2% and 4.9%, respectively (Figure 6A2 and B2), which is similar to the percentages observed for cells exposed to IR. Notably, the proportions of cells at the later division steps (patterns d and e) increased to 8.6% and 10.4%, respectively, indicating a slow kinetics in constriction and separation. Moreover, the dividing cells exposed to IR separated horizontally with angles less than 25 degrees in most cases (Figure 6A1, panels Ld and Le, and D1), whereas cells were often bent at the septa with larger angles in darkness (Figure 6A2, panels Dd and De, and D2). This result suggests a more challenging division process in the dark. Overall, these results indicate that exposure to IR resulted in a smoother division process.

The sixth pattern comprised cells with multiple fluorescence foci, indicating dispersed synthesis or repair of the PG network. This might also suggest difficulties in determining the initiation site for septum synthesis in these cells. When exposed to IR, only 1.4% of cells exhibited multiple fluorescence

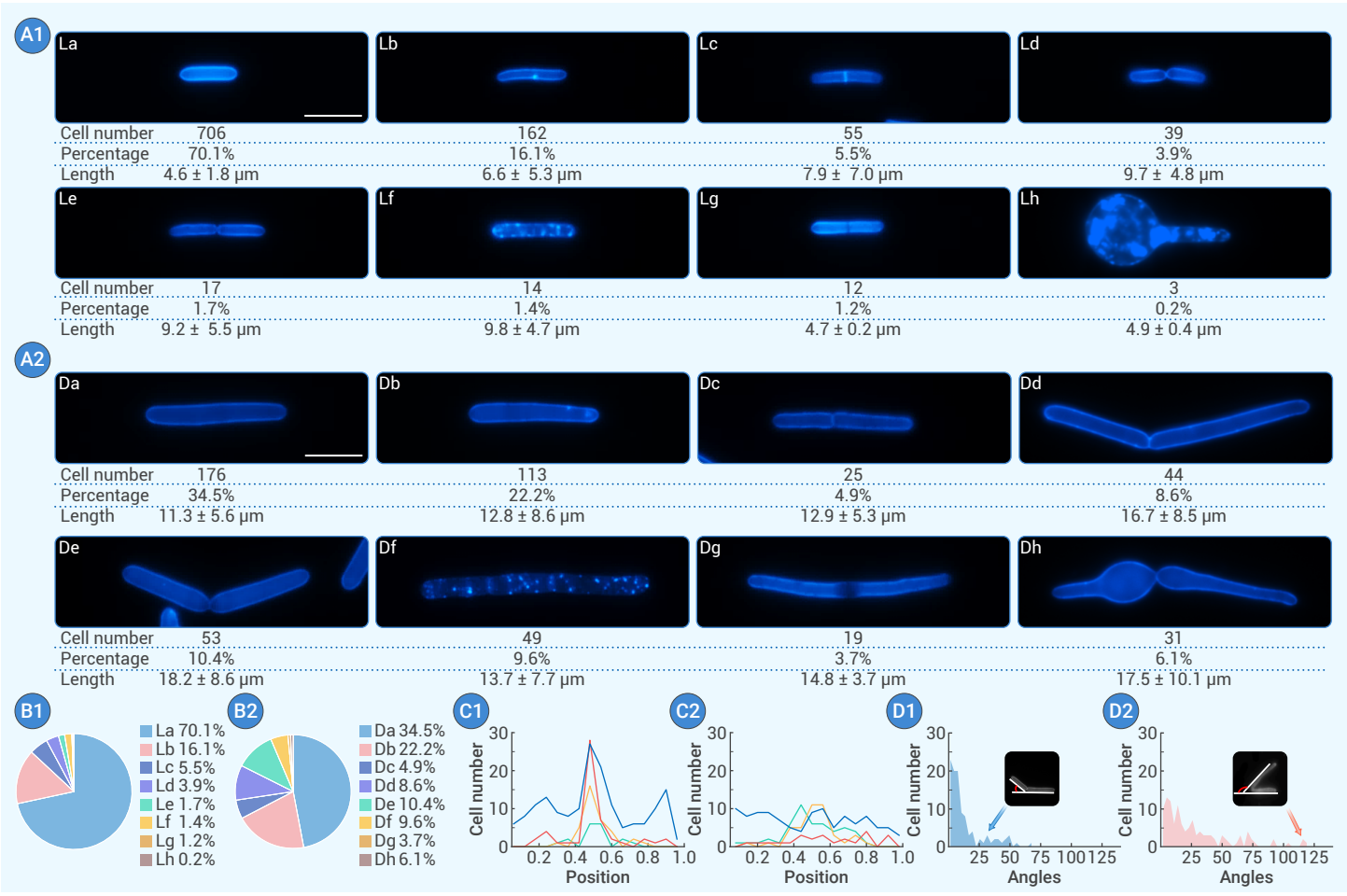


**Figure 6. Patterns of PG synthesis in SWIR-1 cells under HHP at 30 MPa** A1, B1, C1 and D1 are cells exposed to IR irradiation, whereas A2, B2, C2 and D2 are cultures in the dark. A1 and A2 show PG synthesis with HADA 0.2 mM for 20 h. B1 and B2 show the distributions of the 8 patterns of cells. C1 and C2 indicate location of initiation and formation of septa alone the long axis of cells. D1 and D2 are the bending angles of cells in division. Scale bars: 5 μm.

foci, whereas this percentage increased to 9.6% in the dark (Figure 6A-B). The seventh pattern displayed long filaments with the removal of HDAA labeling at the mid-cell, resulting in a sharp unlabeled band in cells exposed to IR and a relatively wider zone in cells incubated in the dark. This observation suggests the removal of PG at these positions (Figure 6A1, Lg, and A2, Dg). The final pattern involved cells with swollen ends (Lh and Dh). Exposure to IR resulted in a negligible proportion of swollen cells (0.2%) compared to a higher proportion (6.1%) observed in darkness. Notably, the beneficial effect of 880 nm irradiance on cell division under HHP was not observed with 970 nm IR at the same radiance.

## DISCUSSION

Bacteria have evolved various mechanisms to adapt and thrive in deep-sea habitats characterized by HHP. The synthesis of peptidoglycan (PG) for cell elongation and division while maintaining cell envelope integrity is a highly challenging process under elevated pressure conditions. In this study, we observed that HHP at certain extent impairs septal PG synthesis and cell division, but not elongation, in the SWIR-1 strain isolated from a deep-sea hydrothermal vent. Remarkably, IR radiation, which is the primary light source emitted by the superhot active black chimney, can trigger septal PG synthesis and alleviate the hindrance of HHP on cell division. Therefore, it appears that the target of HHP and IR irradiation is the divisome-mediated PG synthesis and cell division process.

Genes that have functional relationships or physically interactions often cluster together, which facilitates the sharing of regulatory mechanisms. Notably, genes responsible for critical processes in PG synthesis and bacterial cytokinesis are typically located within a division and cell wall (DCW) gene cluster, a feature conserved in terms of both gene content and gene order across bacterial species.[28] For instance, in the case of *B. subtilis*, the DCW cluster comprises 18 genes (see Figure 7). The *murBGDE* and *mraYZ* genes play essential roles in the synthesis and export of PG precursors. Meanwhile, *ftsZAQWIL* genes are key components of the divisome complex, which is necessary for septal PG synthesis, septa formation, and cell wall constriction. It is worth noting that the *ftsA* gene is typically located adjacent to *ftsZ* in the DCW cluster when present. However, in strain SWIR-1, it was conspicuously absent from the DCW cluster, with its homolog *sepF* found alone at a distal position in the genome (Figure 7).

To gain more insight into the genomic context of the DCW cluster, we conducted a GeCoViz analysis. Using SWIR-1 FtsZ as a query, a sequence search in GeCoViz assigned it to the orthologous group COG0206, which is a critical cell division protein forming the Z-ring. An analysis of the 56 *ftsZ* genes from 47 representative species revealed closely co-localized orthologous groups, including COG1589 FtsQ (VCS 0.66), COG0771 MurD (VCS 0.61), and COG0472 MraY (VCS 0.61). FtsA in COG0849 was found in 51% of these genomes.

The SWIR-1 DCW cluster contains *sbp* and two homologous *ylxW/ylxX* genes directly upstream of *ftsZ*. These three genes are present in the minimal genome of *B. subtilis* strain PG38,[29] suggesting their indispensable function in *B. subtilis*. A similar *ylx-sbp-ftsZ* context was found in the genomes of four species: *Ezakiella massiliensis*, *Veillonella magna* DSM19857, *Eubacteriaceae bacterium* CHKC1005, and *Clostridium formicaceticum* (Figure 7). These four species, including strain SWIR-1, and *B. subtilis* all belong to the Bacillota phylum, suggesting the conservation of the *ylx-sbp-ftsZ* context in this gram-positive phylum. Sbp (small basic protein) belongs to COG3856 PFAM DUF1290, and Ylx belongs to COG3879 of unknown function (DUF881). Further exploration of COG3856 revealed that Sbp has 3,186 orthologs from 1,521 representative species and is embedded in the *ylx-sbp-ftsA/ftsZ* context. Using YlxX as a query in sequence search, we found 8,134

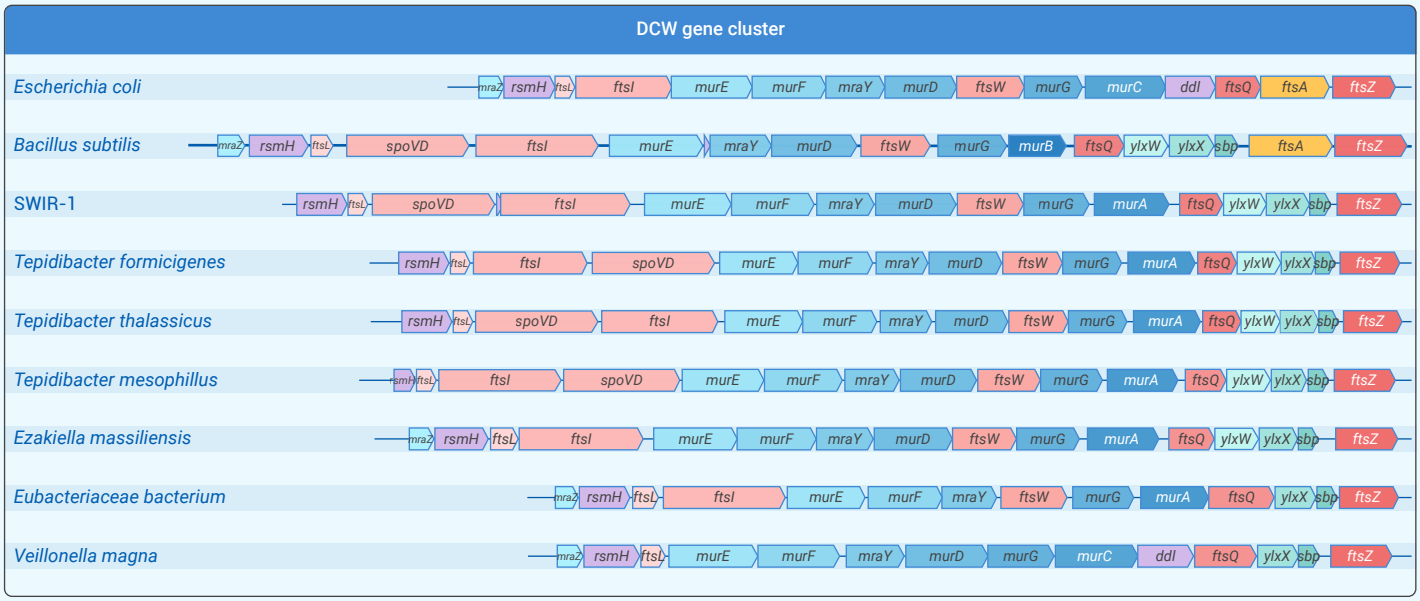


**Figure 7. DCW cluster gene composition** DCW clusters from the gram-negative model strain *E. coli*, gram-positive model strain *B. subtilis*, the strain SWIR-1, as well as those with similar genomic context sorted out by GeCoViz platform are presented.

orthologous proteins in 1,535 representative species. These proteins were closely linked to *sbp* and *fts* genes, suggesting that three proteins likely play a significant role in the cell division process. However, whether these functionally unknown proteins respond to IR irradiation remains unknown.

Expanding on this line of inquiry, it is imperative to conduct comprehensive investigations to determine whether elevated pressure has a widespread impact on the impairment of PG synthesis at septa across various bacterial taxonomy groups. Furthermore, it is crucial to determine if this impairment can be effectively restored through IR irradiation. Since *T. hydrothermalis* SWIR-1 is an obligate anaerobic strain and lacks genetic tools for direct study, a synthetic biology approach using *B. subtilis* or other model cells may help circumvent this obstacle.

The inherent properties of IR light, including its ability to penetrate deep into tissues and its minimal photo-cytotoxic effects, make it a highly promising tool in biomedical applications such as low-level laser (or light) therapy (LLLT). LLLT, also known as photobiomodulation (PBM), uses low levels of red or IR light to stimulate cellular function and treat various conditions like pain, inflammation, wound healing and brain disorders.[30-33] While the mechanism of near-infrared (NIR) PBM is complex and not yet fully understood, several hypotheses have been proposed to explain its effects. One hypothesis is based on the enhancement of enzymatic activities. NIR light at about 850 nm stimulates the activity of mitochondrial enzyme cytochrome c oxidase (CCO), which enhances the electron transport chain, thereby increasing cellular energy production (ATP synthesis) and improving cellular metabolism. In a different range, IR light at 980 nm or longer wavelengths is absorbed by nanostructured water clusters surrounding transient receptor potential (TRPV1) heat/light-gated ion channels. A slight nano- or microscale temperature change triggers a conformational shift in TRPV1, leading to the influx of calcium ions, neuronal depolarization, and the perception of heat.[31,34] Despite the growing number of successful cases in PBM, skepticism persists, impeding its widespread adoption in clinical practice. This is due to the limited understanding of the molecular, cellular, and tissue-level mechanisms underlying the positive outcomes associated with PBM.

Bacteria exhibit varying degrees of absorption of IR radiation, depending on the wavelength and cellular composition. This absorption is primarily due to specific molecular groups and compounds within the bacterial cellular structure. Bacterial cells contain a significant amount of water, and a prominent absorption peak at 976 nm was observed in both water and growth media. Consequently, NIR radiation at this wavelength can induce a thermal effect on bacterial cells. The study investigated the effect of 880 nm and 970 nm on triggering septal PG synthesis and cell division of SWIR-1 under elevated pressure. Only 880 nm but not 970 nm LED could alleviate the inhibition of cell division. It is worth noting that the genome of SWIR-1 code for neither cytochrome c oxidase nor known heat/light-gated ion channels, but encodes copper-containing proteins of unknown function. Further investigation is required to determine whether these proteins are involved in IR-triggered SWIR-1 growth and cell division.

## DECLARATION OF AI-ASSISTED TECHNOLOGIES

During the preparation of this work, the authors used ChatGPT and DeepL to check and improve the English of the manuscript, which was completely written by authors. After using these tools, the authors reviewed and edited the content as necessary and take full responsibility for the content of the publication.

## REFERENCES


1. Du, M., Peng, X., Zhang, H., et al. (2021). Geology, environment, and life in the deepest part of the world's oceans. Innovation (Camb) **2**(2): 100109. DOI: 10.1016/j.xinn.2021.100109.
2. Bartlett, D.H. (2002). Pressure effects on in vivo microbial processes. Biochim Biophys Acta **1595**(1-2): 367–381. DOI: 10.1016/s0167-4838(01)00357-0.
3. Oger, P.M., and Jebbar, M. (2010). The many ways of coping with pressure. Research in Microbiology **161**(10): 799–799. DOI: 10.1016/j.resmic.2010.09.017.
4. Black, S.L., Dawson, A., Ward, F.B., and Allen, R.J. (2013). Genes Required for Growth at High Hydrostatic Pressure in *Escherichia coli* K-12 Identified by Genome-Wide Screening. PloS one **8**(9): e73995. DOI: 10.1371/journal.pone.0073995.
5. Li, A.Q., Zhang, W.J., Li, X.G., et al. (2023). Piezophilic Phenotype Is Growth Condition Dependent and Correlated with the Regulation of Two Sets of ATPase in Deep-Sea Piezophilic Bacterium *Photobacterium profundum* SS9. Microorganisms **11**(3). DOI: 10.3390/microorganisms11030637.
6. Yin, Q.J., Zhang, W.J., Qi, X.Q., et al. (2018). High hydrostatic pressure inducible trimethylamine N-oxide reductase iImproves the pressure tolerance of piezosensitive bacteria *Vibrio fluvialis*. Front Microbiol **8**: 2646. DOI: 10.3389/fmicb.2017.02646.
7. Zobell, C.E., and Oppenheimer, C.H. (1950). Some effects of hydrostatic pressure on the multiplication and morphology of marine bacteria. J Bacteriol **60**(6): 771–781. DOI: 10.1128/jb.60.6.771-781.1950.
8. Zobell, C.E., and Cobet, A.B. (1964). Filament formation by *Escherichia coli* at increased hydrostatic pressure. J Bacteriol **87**(3): 710–719. DOI: 10.1128/jb.87.3.710-719.1964.
9. Ishii, A., Sato, T., Wachi, M., et al. (2004). Effects of high hydrostatic pressure on bacterial cytoskeleton FtsZ polymers in vivo and in vitro. Microbiology **150**(Pt 6):1965-1972. DOI: 10.1099/mic.0.26962-0.
10. Dick, G.J. (2019). The microbiomes of deep-sea hydrothermal vents: distributed globally, shaped locally. Nat Rev Microbiol **17**(5): 271–283. DOI: 10.1038/s41579-019-0160-2.
11. He, X., Xu, T., Chen, C., et al. (2023). Same (sea) bed different dreams: Biological

community structure of the Haima seep reveals distinct biogeographic affinities. The Innovation Geoscience **1**(2): 100019. DOI: 10.59717/j.xinn-geo.2023.100019.
12. Van Dover, C.L., Reynolds, G.T., Chave, A.D., and Tyson, J.A. (1996). Light at deep-sea hydrothermal vents. Geophys. Res. Lett. **23**(16): 2049–2015. DOI: 10.1029/96GL02151.
13. Nisbet, E.G., Cann, J.R., and Van Dover, C.L. (1995). Origins of photosynthesis. Nature **373**: 479–480. DOI: 10.1038/373479a0.
14. Martin, W.F., Bryant, D.A., and Beatty, J.T. (2018). A physiological perspective on the origin and evolution of photosynthesis. FEMS Microbiol Rev **42**(2): 205–231. DOI: 10.1093/femsre/fux056.
15. Xiao, W., He, H., Li, Y., and Konhauser, K. (2023). Abiotic oxidants promoted cyanobacteria's evolution and Earth's oxidation. The Innovation Geoscience **1**: 100003. DOI: 10.59717/j.xinn-geo.2023.100003.
16. Yurkov, V.V., Krieger, S., Stackebrandt, E., and Beatty, J.T. (1999). *Citromicrobium bathyomarinum*, a novel aerobic bacterium isolated from deep-sea hydrothermal vent plume waters that contains photosynthetic pigment-protein complexes. J Bacteriol **181**(15): 4517–4525. DOI: 10.1128/JB.181.15.4517-4525.1999.
17. Beatty, J.T., Overmann, J., Lince, M.T., et al. (2005). An obligately photosynthetic bacterial anaerobe from a deep-sea hydrothermal vent. Proceedings of the National Academy of Sciences of the United States of America **102**(26): 9306–9310. DOI: 10.1073/pnas.0503674102.
18. Chen, H., Li, D.H., Jiang, A.J., et al. (2022). Metagenomic analysis reveals wide distribution of phototrophic bacteria in hydrothermal vents on the ultraslow-spreading Southwest Indian Ridge. Marine Life Science & Technology **4**(2): 255–267. DOI: 10.1007/s42995-021-00121-y.
19. Dai, J., Li, X.G., Zhang, W.J., and Wu, L.F. (2023). *Tepidibacter hydrothermalis* sp. nov., a novel anaerobic bacterium isolated from a deep-sea hydrothermal vent. Int J Syst Evol Microbiol **73**(11). DOI: 10.1099/ijsem.0.006151.
20. Cutler, K.J., Stringer, C., Lo, T.W., et al. (2022). Omnipose: a high-precision morphology-independent solution for bacterial cell segmentation. Nature Methods **19**(11): 1438–1448. DOI: 10.1038/s41592-022-01639-4.
21. Koch, E.W., and Rosolowsky, E.W. (2015). Filament Identification through Mathematical Morphology. arXiv **1507**: 02289. DOI: 10.48550/arXiv.1507.02289.
22. Du, P., Kibbe, W.A., and Lin, S.M. (2006). Improved peak detection in mass spectrum by incorporating continuous wavelet transform-based pattern matching. Bioinformatics **22**(17): 2059–2065. DOI: 10.1093/bioinformatics/btl355.
23. Botas, J., Rodríguez del Río, Á., Giner-Lamia, J., and Huerta-Cepas, J. (2022). GeCoViz: genomic context visualisation of prokaryotic genes from a functional and evolutionary perspective. Nucleic Acids Research **50**(W1): W352–W357. DOI: 10.1093/nar/gkac367.
24. Li, X.-G., Dai, J., Zhang, W.-J., et al. (2023). Genome analysis of *Tepidibacter* sp. SWIR-1, an anaerobic endospore-forming bacterium isolated from a deep-sea hydrothermal vent. Marine Genomics **71**: 101049. DOI: 10.1016/j.margen.2023.101049.
25. Egan, A.J.F., Errington, J., and Vollmer, W. (2020). Regulation of peptidoglycan synthesis and remodelling. Nat Rev Microbiol **18**(8): 446–460. DOI: 10.1038/s41579-020-0366-3.
26. Kuru, E., Tekkam, S., Hall, E., et al. (2015). Synthesis of fluorescent D-amino acids and their use for probing peptidoglycan synthesis and bacterial growth in situ. Nat Protoc **10**(1): 33–52. DOI: 10.1038/nprot.2014.197.
27. Hsu, Y.P., Rittichier, J., Kuru, E., et al. (2017). Full color palette of fluorescent d-amino acids for in situ labeling of bacterial cell walls. Chem Sci **8**(9): 6313–6321. DOI: 10.1039/c7sc01800b.
28. Megrian, D., Taib, N., Jaffe, A.L., et al. (2022). Ancient origin and constrained evolution of the division and cell wall gene cluster in Bacteria. Nature Microbiology **7**(12): 2114–2127. DOI: 10.1038/s41564-022-01257-y.
29. Michalik, S., Reder, A., Richts, B., et al. (2021). The Bacillus subtilis Minimal Genome Compendium. ACS Synthetic Biology **10**(10): 2767–2771. DOI: 10.1021/acssynbio.1c00339.
30. Tsai, S.R., and Hamblin, M.R. (2017). Biological effects and medical applications of infrared radiation. J Photochem Photobiol B **170**: 197–207. DOI: 10.1016/j.jphotobiol.2017.04.014.
31. Sharma, S.K., Sardana, S., and Hamblin, M.R. (2023). Role of opsins and light or heat activated transient receptor potential ion channels in the mechanisms of photobiomodulation and infrared therapy. Journal of Photochemistry and Photobiology **13**: 100160. DOI: 10.1016/j.jpap.2023.100160.
32. Dai, H., Shen, Q., Shao, J., et al. (2021). Small Molecular NIR-II Fluorophores for Cancer Phototheranostics. Innovation (Camb) **2**(1): 100082. DOI: 10.1016/j.xinn.2021.100082.
33. Zhou, Y., Li, J., Tan, Q., et al. (2023). Soft electronics go for three-dimensional health monitoring in deep tissue. The Innovation Materials **1**(2): 100022. DOI: 10.59717/j.xinn-mater.2023.100022.
34. Hamblin, M.R., Huang, Y.Y., and Heiskanen, V. (2019). Non-mammalian Hosts and Photobiomodulation: Do All Life-forms Respond to Light. Photochem Photobiol **95**(1): 126–139. DOI: 10.1111/php.12951.

## ACKNOWLEDGMENTS

We would like to express our grateful to all the participants of the TS10-1/-2 cruise, the captain and crew of the R/V "Tan Suo Yi Hao" and pilots of the submersible "Shen Hai Yong Shi" for their professional service during this cruise. We also thank K. Ding for valuable advice about hydrothermal vent light emission and K. Ding and X. Peng[s'] help for diving and sampling, A. Grossi for conception and mounting LED and HPOU to ZEISS microscope, H. Le Guenno and L. Espinosa for microscopy assistance. This research was funded by grants NSFC 42176121, 42076127, U2106228 and 92351304 from the National Natural Science Foundation of China, grants DBM 2021, DBM 2023 and LIA-MagMC from the Centre National de la Recherche Scientifique, grants 2018YFC0309904 and 2016YFC0304905 from Ministry of Science and Technology of China, and grants ZDKJ2021028 and ZDKJ2019011 from the Major Scientific and Technological Projects of Hainan Province. J.D. was supported by China Scholarship Council and T.Y. Zhang was sponsored by Institute of Cancer and Immunology and Aix-Marseille University.

## AUTHOR CONTRIBUTIONS

L.F. Wu designed and supervised the study; L.F. Wu, X.G. Li and W.J. zhang collected the sample; L.F. Wu, X.G. Li, J.D. and Y.L. enriched microorganisms from sample; X.G. Li isolated the strain SWIR-1; L.F. Wu, J.D., X.G. Li and H.C. performed the high hydrostatic pressure incubation and infrared irradiated incubation; J.D. performed the microscope images analysis, T.Y. Zhang designed the image analysis tool; D.H. Li and J.W. Chen analyzed the metagenomic data; J.L. designed the graphic abstract; L.F. Wu, J.D., X.G. Li and W.J. Zhang drafted the manuscript and designed the figures. All authors discussed the results and commented on the manuscript.

## DECLARATION OF INTERESTS

The authors declare no competing interests.

## SUPPLEMENTAL INFORMATION

It can be found online at https://doi.org/10.59717/j.xinn-geo.2024.100050

The Innovation Geoscicence, *Volume 2*

# Supplemental Information

## Illuminating a bacterial adaptation mechanism: Infrared-driven cell division in deep-sea hydrothermal vent environments

**DOI:** https://doi.org/10.59717/j.xinn-geo.2024.100050

Jie Dai, Xue-Gong Li, Tian-Yuan Zhang, Hong Chen, Wei-Jia Zhang, Denghui Li, Jia Liu, Jianwei Chen, Yuan Lu, and Long-Fei Wu

# Table of Contents

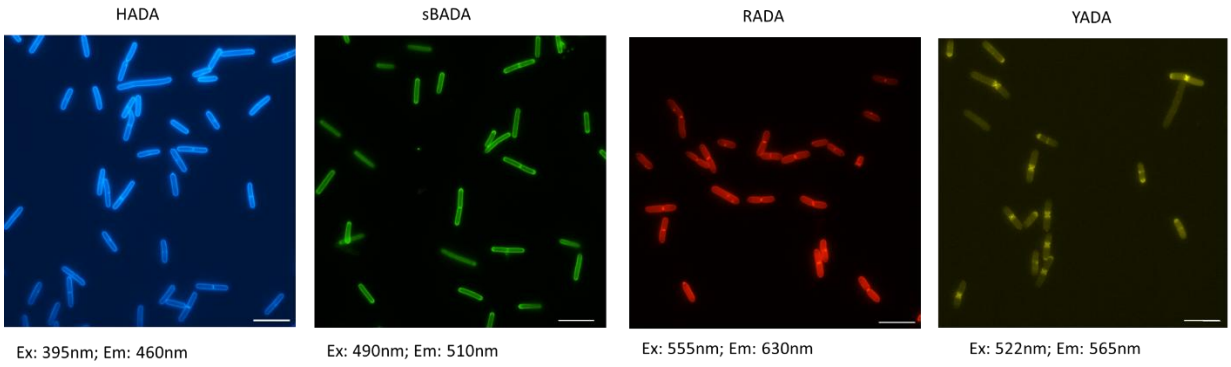


**Figure S1** FDAA incorporation in SWIR-1 cell wall. SWIR-1 cells were incubated with one of four FDAA at final concentration of 0.2 mM under anaerobic conditions. Scale bars equal 5 μm.

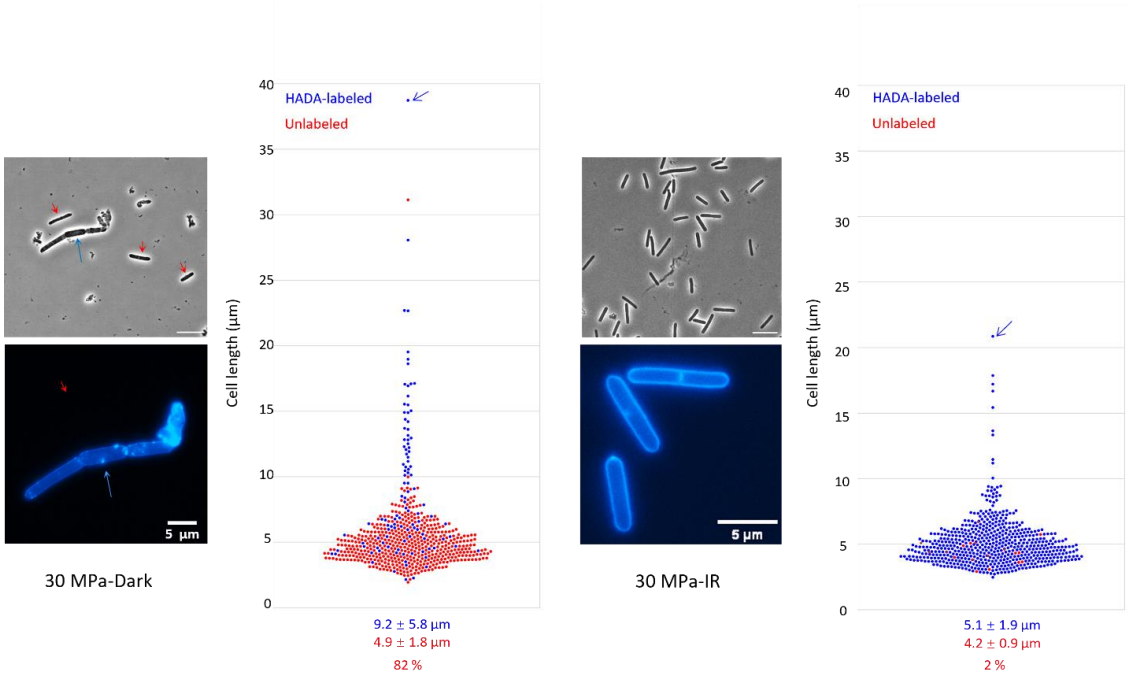


**Figure S2** Distribution of size and PG synthesis of cells incubated under elevated pressure in darkness or with IR irradiation. Red arrows indicated labelling inert cells that were represented by red spots and red numbers in swarm plot. Blue arrows indicate the longest filamentous cells. Scale bars: 5 μm.

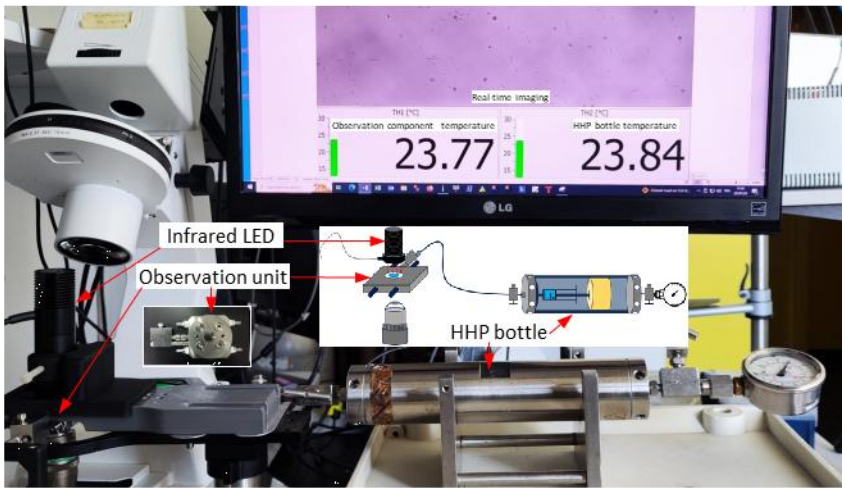


**Figure S3** Schematic presentation of High-Pressure Cell Growth Analysis Device (HPCG). The High-pressure observation unit (HPOU) is connected to a high-pressure bottle and is mounted onto a microscope plate. An LED light has been added to illuminate the HPOU, and the imaging is displayed on the computer screen. Additionally, temperature readings from the HPOU and the pressure cylinder are shown on the screen.